Journal of Hazardous Materials 182 (2010) 123–129

Contents lists available at ScienceDirect

Journal of Hazardous Materials

journal homepage: www.elsevier.com/locate/jhazmat

Synthesis of Ag/ZnO nanorods array with enhanced photocatalytic performance

Chunlei Ren, Beifang Yang*, Min Wu, Jiao Xu, Zhengping Fu, Yan lv, Ting Guo, Yongxun Zhao, Changqiong Zhu

CAS Key Laboratory of Materials for Energy Conversion, Department of Materials Science and Engineering, University of Science and Technology of China, Hefei, Anhui 230026, PR China

ARTICLE INFO

Article history:
Received 24 February 2010
Received in revised form 12 May 2010
Accepted 31 May 2010
Available online 8 June 2010

Keywords:
Ag
ZnO
Nanorods array
Photo deposition
Photocatalytic activity

ABSTRACT

Silver-modified ZnO nanorods array has been prepared and the effect of silver modification has been studied. ZnO nanorods array were fabricated through a wet chemical route and a photo deposition method was taken to fabricate silver nano particulate on the ZnO nanorods. The structural and optical properties were characterized by field emission scanning electron microscope, high resolution transmission electron microscope, X-ray photoelectron spectroscopy, Raman, UV–vis and photoluminescence (PL) spectra. The UV photocatalytic activity of these materials was studied by analyzing the degradation of methylene blue (MB) in aqueous solution. The photocatalytic performance indicated that Ag deposit acted as not only electron sinks to enhance the separation of photoexcited electrons from holes, but also charge carrier recombination centers, so the optimized amount of Ag deposit was investigated.

1. Introduction

Aside from TiO_2, ZnO is one of the most promising materials for remediation of contaminants and destruction of microorganisms. Both materials exhibit very similar band gaps (ZnO, 3.37 eV; TiO_2, 3.2 eV) and conduction band edge positions [1]. These semiconductors are well established and there has been considerable interest in their applications to the area of photocatalysis [2]. The general scheme for the photocatalytic destruction of organic compounds involves the following three steps: (i) when the energy $h\upsilon$ of a photon is equal to or higher than the band gap (E_g) of the semiconductor, an electron is excited to CB, with simultaneous generation of a hole in the VB; (ii) then the photoexcited electrons and holes can be trapped by the oxygen and surface hydroxyl, respectively, to ultimately produce the hydroxyl radicals (•OH), which are known as the primary oxidizing species; and (iii) the hydroxyl radicals commonly mineralize the adsorbed organic substances.

However, the photoexited electrons and holes can also recombine to reduce photocatalytic activity of the semiconductor. To overcome this limitation, modification of semiconductors with noble metals is one of the most efficient ways [3,4]. ZnO/Ag composite structure is now an exciting area in research for developing photocatalytic applications. Ag is known as electron sinks due to the Schottky barrier at the metal-semiconductor interface [5,6], then after step (i) as mentioned above, electron in CB can transfer to Ag deposit.

Although there are reports about the effect of silver addition in the electronic and optical properties of ZnO [7–10], to the best of our knowledge, there are no detailed studies on the effect of silver modification in ZnO nanorods array, especially photocatalytic activity. Compare with 0D and 2D nanostructures, 1D systems, such as nanowires and nanorods, are the smallest dimension structures that can be used for efficient transport of electrons and optical excitations, and are thus expected to be critical to the function and integration of nanoscale devices [11]. Moreover, ZnO nanorods array displays a broadband reflection suppression from 400 to 1200 nm [12]. In this work, we report a systematic study on the effect of modification on ZnO nanorods array with various amounts of silver nanoparticles for the photocatalytic activity of ZnO nanorods array.

2. Experimental

2.1. Preparation of ZnO/Ag nanorods array

To fabricate ZnO/Ag structure, zinc acetate dehydrate and silver nitrate were used as Zn and Ag sources, respectively. All chemicals were of analytical reagent grade and used without further purification.

As shown in Scheme 1, ZnO nanorods array (ZnO NRA) on the glass substrate were prepared through a typical two-step method [13,14]. Briefly, ZnO seed layers were firstly deposited on glass

* Corresponding author.
E-mail address: bfyang@ustc.edu.cn (B. Yang).

0304-3894/$ – see front matter © 2010 Elsevier B.V. All rights reserved.
doi:10.1016/j.jhazmat.2010.05.141

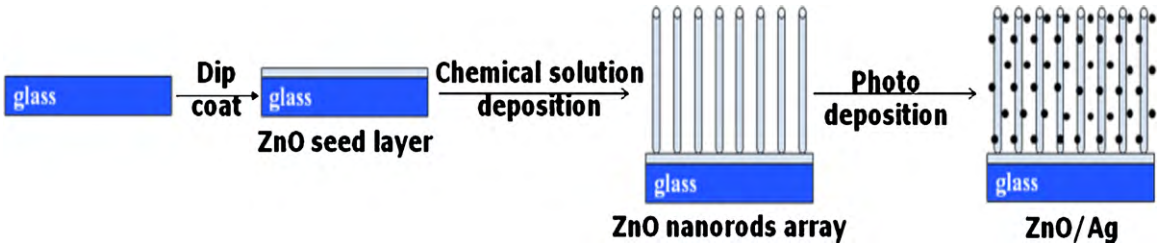

Scheme 1. Scheme illustration of the synthesis steps of Ag/ZnO NRA.

substrates using the dip coating method [15], precursor solutions for the aqueous solution growth were prepared by dissolving zinc acetate dehydrate [$Zn(Ac)_2{\cdot}2H_2O$] and hexamethylenetetramine ($C_6H_{12}N_4$) in deionized water. The concentration of zinc and amine were fixed at 0.02 mol/L. ZnO-coated substrates were suspended in the precursor solutions at 90 °C for 1.5 h without any stirring. Subsequently, the resultant films were thoroughly washed with deionized water to remove any residual salt or amino complex and dried in air at room temperature.

Ag nanoparticles dispersed on ZnO nanorods were prepared by photo deposition method [16,17], and the amount of Ag in each sample was controlled by the concentration of $AgNO_3$ solution, with the settled adsorption time and UV irradiation time. The as-prepared ZnO nanorods array were pre-irradiated with UV-light (main wavelength: 254 nm, 1.9 mW/cm^2) for 1 h to enhance its hydrophility and then soaked in $AgNO_3$ aqueous solution with different concentration (0.02–0.2 mol/L) for 1 h to allow complete adsorption of Ag^+ ions onto ZnO surface. After being rinsed with pure water and dried at room temperature, the film was irradiated with a 20 W low-pressure mercury lamp (main wavelength: 254 nm, 1.9 mW/cm^2) for 20 min to reduce adsorbed Ag^+ to Ag nanoparticles and then washed with deionized water repeatedly to remove the residual Ag^+. The mechanism was shown in Scheme 2. Silver-modified ZnO seed layer films were also obtained by the photo deposition method as mentioned above, without the aqueous solution growth process of ZnO NRA.

2.2. Sample characterizations

To characterize the morphologies of the as-prepared samples, FESEM (JSM-6700F), TEM (JEOL-2010) and HRTEM (JEOL-2010) were obtained. Raman analysis (LABRAM-HR, 514.5 nm Ar^+ pump laser) has been carried out to assess the crystal phase. In order to study the optical properties, UV–vis absorption spectra were measured by an UV–vis spectrophotometer (Shimadzu UV-2401). The surface property was determined by XPS (Thermo Electron ESCALAB-250). The photoluminescence (PL) spectra of the samples were measured with spectrophotometer (Hitachi F-4600) by using 325 nm line of Xe lamp as excitation source at room temperature.

2.3. Photocatalytic studies

For photocatalytic activity studies, samples with the same thickness and geometric area (1 cm × 2 cm) were settled in a 15 mL methylene blue (MB) aqueous solution with a concentration of 2 mg/L in a glass cell, and the ultraviolet light was provided by a low-pressure fluorescent Hg lamp (main wavelength: 254 nm, 1.9 mW/cm^2). Prior to irradiation, the samples were immersed in the same solution for 0.5 h in darkness to establish a adsorption equilibrium. The residual concentration of MB after irradiation for a definite time was estimated according to the absorbance at 662 nm measured by UV–vis spectrophotometer.

3. Results and discussion

3.1. Morphologies observation

The representative FESEM image of ZnO sample shown in Fig. 1 reveals well-aligned ZnO nanorods grown on glass substrate. From the top view and side view images, it can be clearly seen that, the diameters of the nanorods ranged from 100 to 125 nm and the length was about 1.0 μm. The diameter and length of nanorods were dependent on the growth parameters such as zinc salt concentration, growth temperature, pH, and zinc seed layer morphology [14,18,19]. Moreover, the diameter distribution of the rods is narrow and the rod density is suitable for silver deposition.

The typical TEM/HRTEM images in Fig. 2 reveal the structure relationship between ZnO rods and silver particulates; the size of Ag particulate in Fig. 2b is bigger than that in Fig. 2a, due to the increase

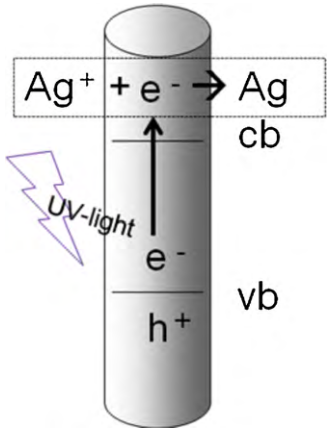

Scheme 2. Charge transfer mechanism of photo deposition method.

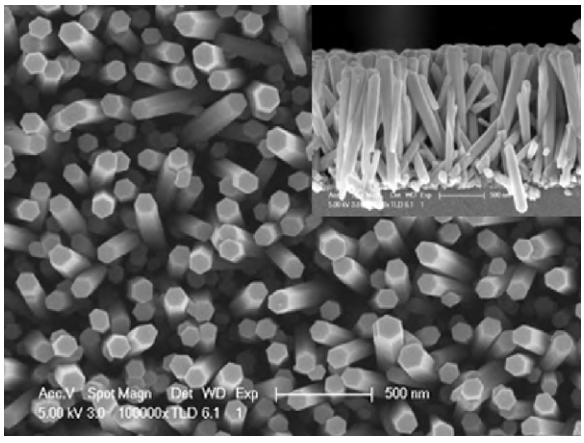

Fig. 1. a top view SEM image of the well-aligned ZnO nanorods array and its cross section (inset).

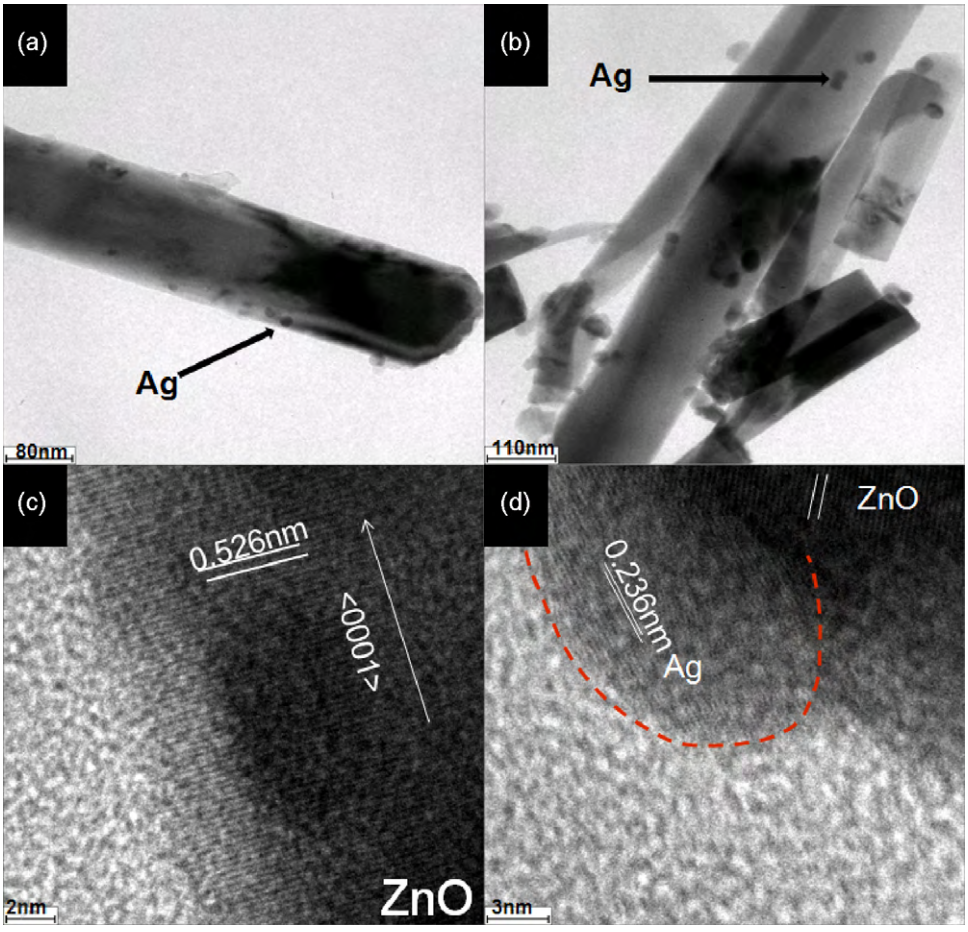

Fig. 2. Typical TEM images of the as-synthesized Ag/ZnO NRA with an $AgNO_3$ concentration of (a) 0.02 M, (b) 0.05 M and (c) HRTEM image of the ZnO, (d) HRTEM image of Ag/ZnO with an $AgNO_3$ concentration of 0.05 M (Ag 0.37 at.%).

of $AgNO_3$ concentration. However, we cannot easily control the distribution of the particle size of Ag, and photo deposition method also has its limitation such as the adhesive capacity of the produced Ag particles is not very good, thus this preparation process needs further improvement. The 2D lattice fringes in the HRTEM images, parts c and d, signify the crystallinity of the ZnO nanorod. The distance between two fringes is about 0.526 nm, which is close to the *d* spacing of the (0 0 0 1) plane, indicating that the ⟨0 0 0 1⟩ direction (*c* axis) is the growth direction of ZnO nanorods. And in Fig. 2d, the lattice fringes with interplanar spacing of 0.236 nm, corresponding to the (1 1 1) plane of crystalline Ag nanoparticles, are also observed. Therefore, highly ordered ZnO nanorods array structure modified with Ag nanoparticles was successfully obtained.

3.2. Raman and UV–vis spectra

To assess the crystal quality, Raman analysis has been carried out on the samples. Raman spectra of ZnO NRA and silver-modified ZnO NRA with $AgNO_3$ of 0.05 M are shown in Fig. 3. The intense peak at 436 cm^{-1} corresponds to E_2 mode of ZnO hexagonal wurtzite structure, and a small peak at 580 cm^{-1} is associated with oxygen deficiency [20,21], revealing the high quality of the ZnO nanorods. Moreover, silver-modified ZnO did not reveal additional modes.

The absorption spectra of unmodified and silver-modified ZnO NRA are presented in Fig. 4 and it can be seen that the pure ZnO (band gap 3.37 eV) showed a steep absorption at wavelength shorter than 380 nm, and the silver addition did not make any significant difference in its band gap. Nevertheless, intense absorption of Ag/ZnO NRA was observed to nearly cover the whole visible region (400–700 nm) due to surface plasmon resonance (SPR) absorption of Ag nanoparticles [22–24]. Furthermore, silver-modified ZnO seed layer films with different contents of Ag were employed to corroborate the SPR absorption of Ag nanoparticles, as showed in Fig. 5. The SPR absorption of Ag nanoparticles was observed as expected. While the concentration of $AgNO_3$ increased, the absorption intensity of the film increased. And we noticed that there were red shifts of resonance peaks (from ~425 to ~463 nm), which was caused by the growth of silver particle size [25].

3.3. XPS analysis

The surface structure of the as-prepared sample with an Ag content of 0.37 at.% (the concentration of $AgNO_3$ aqueous solution is 0.05 M) was investigated by using XPS analysis, and the corresponding experiment results are shown in Fig. 6. The survey spectrum (Fig. 6a) indicates that the sample is composed of Ag, Zn, and O. A weak C emission peak is observed in the spectrum which results from sample holder. No peaks of other elements can be observed. In Fig. 6b, the O 1s profile is asymmetric and can be fitted to two symmetrical peaks (α and β locating at 530.1 and 531.5 eV, respectively), indicating two different kinds of O species in the sample. The peaks α and β should be associated with the lattice oxygen (O_L) of ZnO and chemisorbed oxygen (O_H) caused by the surface hydroxyl [26–28], respectively.

Fig. 6c shows the Ag 3d XPS spectra for the sample. There are two peaks locating at 367.5 and 373.4 eV, which are attributed to Ag $3d_{5/2}$ and Ag $3d_{3/2}$, respectively. Moreover, the binding energy of Ag $3d_{5/2}$ for the Ag/ZnO sample shifts remarkably to the lower

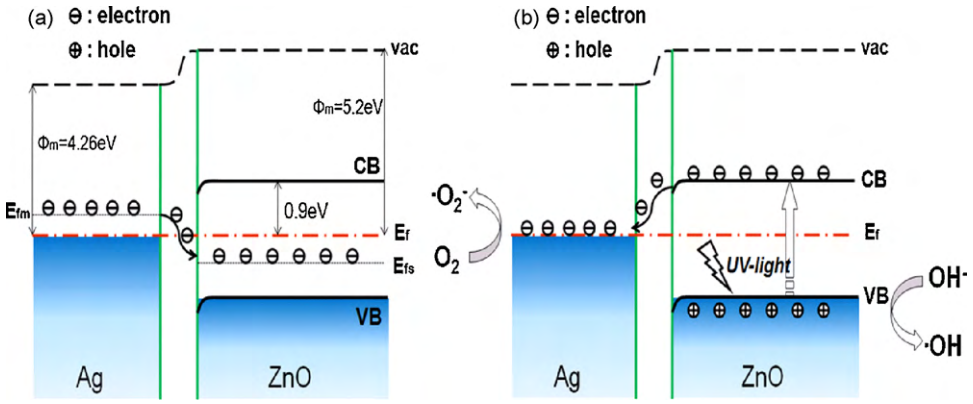

Scheme 3. (a) The band structures of Ag and ZnO junction and the Fermi energy level equilibrium [27–29] without UV irradiation. (b) The proposed charge separation process and the photocatalytic mechanism of as-prepared Ag/ZnO samples under UV irradiation. The electrons in the Ag sinks can be trapped by the chemisorbed O_2 and the hole can be captured by the surface hydroxyl.

binding energy compared with the corresponding value of the synthesized pure metallic Ag (BE value of Ag^0 and Ag^+ is about 368.2 and 367.2 eV, respectively) [29], indicating that the electron density of Ag is decreased. The shift must be due to the strong interaction between Ag and ZnO. Scheme 3a shows the band structures and the Fermi energy levels of Ag and ZnO junction. Because the Fermi energy level of Ag (E_{fm}) is higher than that of ZnO (E_{fs}), part of electrons transferred from Ag to ZnO until the two systems attained equilibrium and a new Fermi energy level (E_f) was formed.

3.4. Photocatalytic performance

We checked the photocatalytic performance of the Ag/ZnO NRA with different Ag contents for degradation of MB. As an example, the time-dependent absorbance spectra of the dye solution are shown in Fig. 7 in the presence of Ag/ZnO NRA with an Ag content of 0.37 at.%. It can be seen that the absorbance peak at 662 nm is reduced significantly, indicating the degradation of the dye molecules. Then the effect of modification with various amounts of silver nanoparticles for the photocatalytic activity of ZnO nanorods array was systematically studied, the photocatalytic experimental data can be converted to a linear pattern using pseudo-first kinetics model, and the results are shown in Fig. 8, the insert shows the photodegradation ratio of different samples after 1 h irradiation. The observed rate constants and photodegradation ratios are calculated as listed in Table 1. It can be seen that the loading of silver can significantly enhance the photocatalytic efficiency of ZnO in degradation of MB. The percentage degradation varied from 36.2% to 49.3% for different concentrations of $AgNO_3$ solution. It can be seen that the photocatalytic activity of these samples vary in the following order: pure ZnO < ZnO/Ag (0.02 M) < ZnO/Ag (0.05 M) > ZnO/Ag (0.1 M) > ZnO/Ag (0.2 M), it is found that the molar content of 0.37%

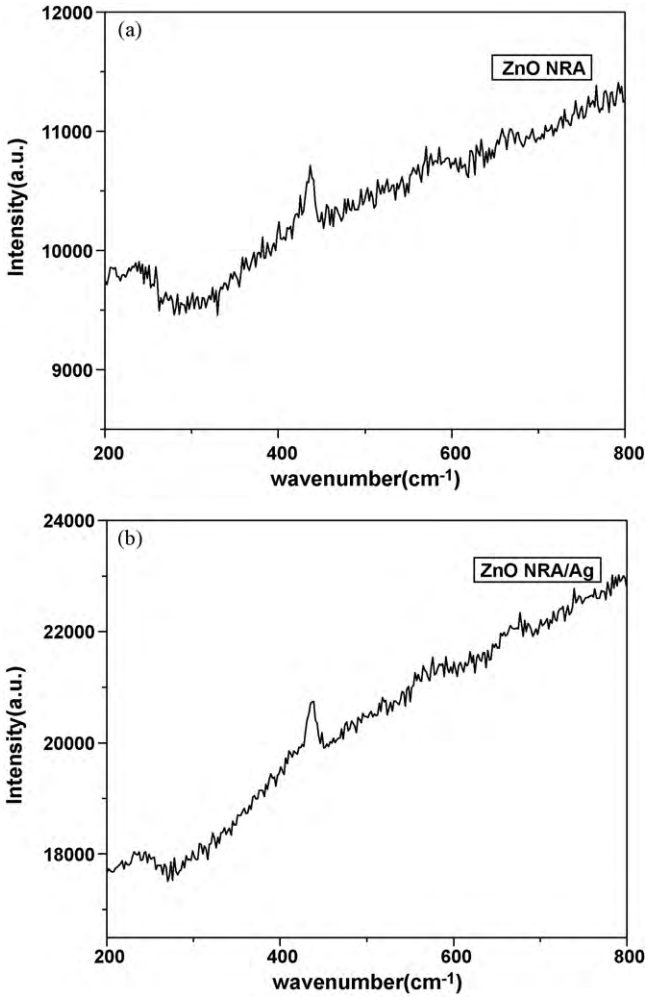

Fig. 3. Resonant Raman spectrum of (a) pure ZnO NRA, (b) Ag/ZnO NRA with an $AgNO_3$ concentration of 0.05 M.

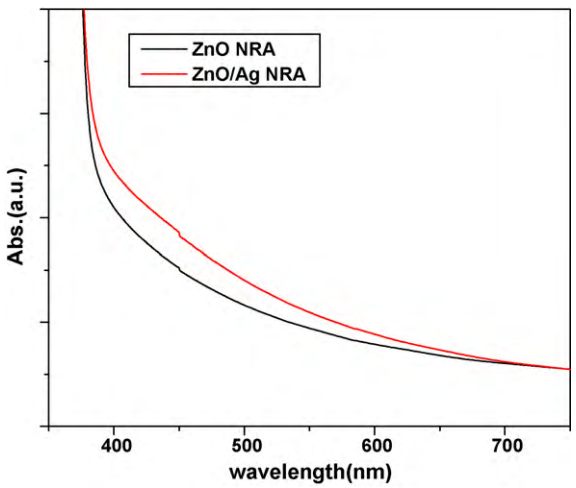

Fig. 4. UV–vis absorption spectrum of pure ZnO NRA (black) and Ag/ZnO NRA (red) with an $AgNO_3$ concentration of 0.05 M (For interpretation of the references to color in this figure legend, the reader is referred to the web version of the article.).

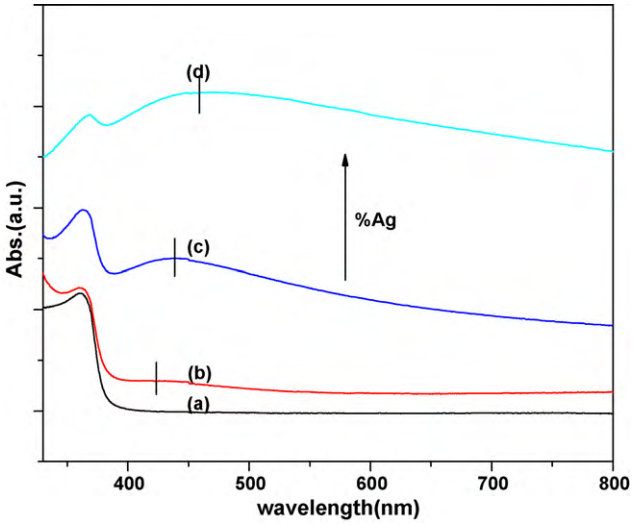

Fig. 5. UV–vis absorption spectrum of (a) pure ZnO seed layer film, and Ag/ZnO film with an $AgNO_3$ concentration of (b) 0.02 M, (c) 0.05 M, (d) 0.2 M.

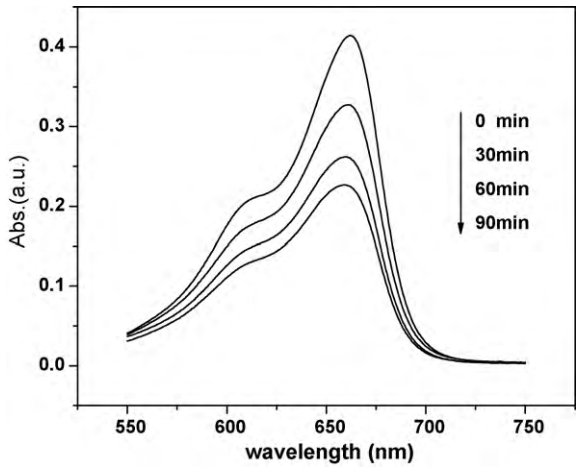

Fig. 7. Time-dependent UV–vis absorbance spectra of the MB solution in the presence of Ag/ZnO sample with an Ag content of 0.37 at.%.

(the concentration of $AgNO_3$ aqueous solution is 0.05 M) is the best dosage to achieve the highest photodegradation rate, so the optimal Ag loading for achieving the highest photocatalytic activity is 0.37 at.%. When the Ag loading is higher than this level, the photocatalytic activity will decrease with increasing Ag loading. The positive effect of noble metal deposits is commonly explained by the opinion that Ag nanoparticles on the semiconductor surface behave like electron sinks, which provide sites for accumulation of the photogenerated electrons, and then improve the separation of electrons and holes. This can be understood based on the pro-

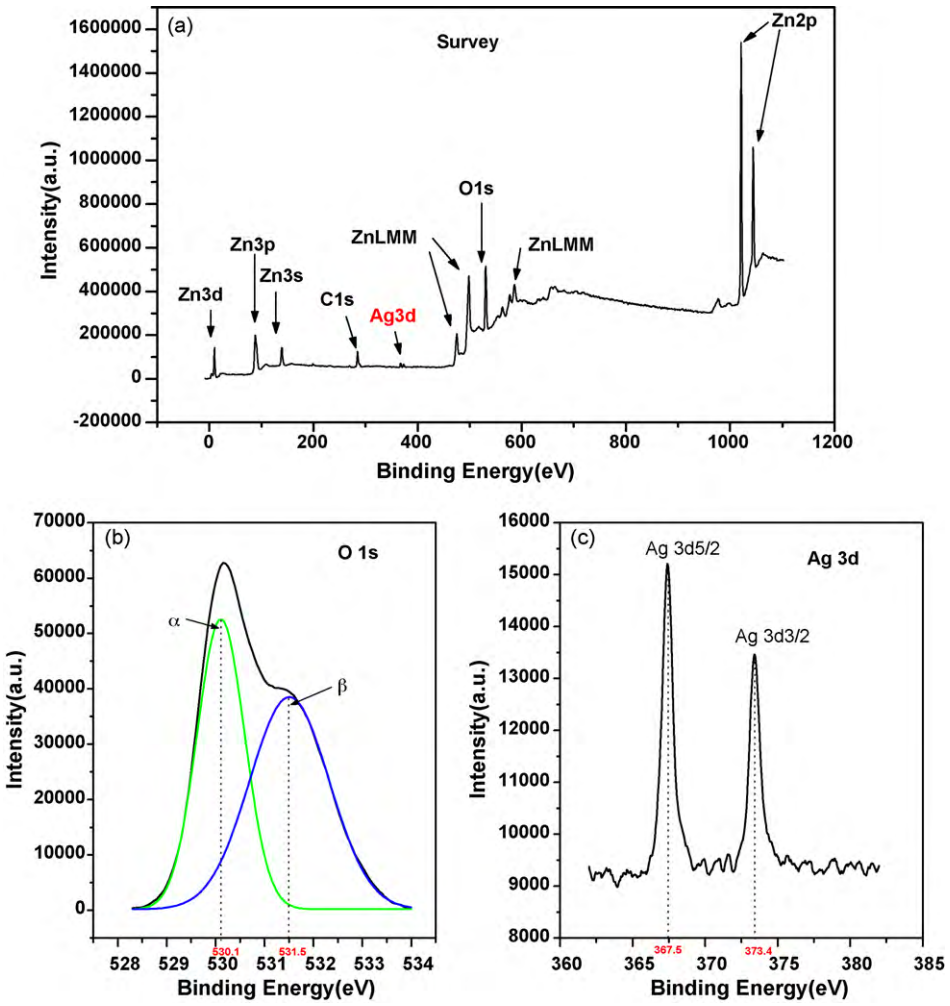

Fig. 6. (a) Representative XPS survey spectrum, (b) XPS full spectra of O 1s, (c) Ag 3d of the as-prepared Ag/ZnO sample with an Ag content of 0.37 at.%.

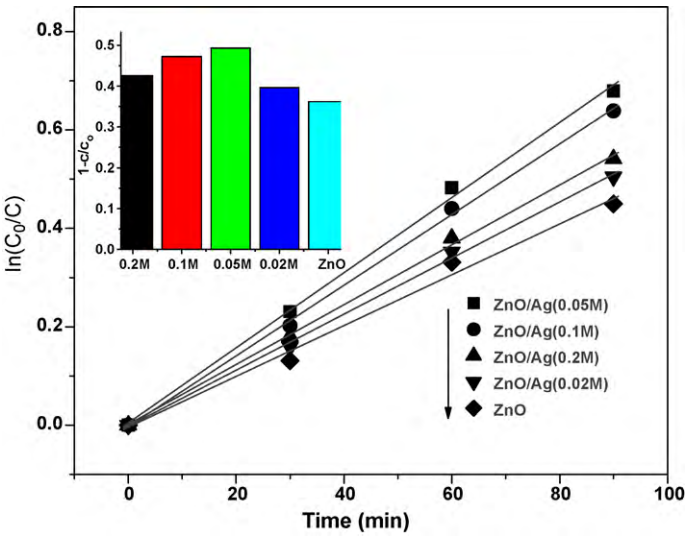

Fig. 8. The $\ln(C_0/C)$ versus time curves of photodegradation of MB. C_0 and C are the initial concentration after the adsorption equilibrium and the reaction concentration of MB, respectively. The experimental data are fitted using the pseudo-first-order kinetic equation: $\ln(C_0/C) = kt$.

posed charge separation of Ag/ZnO under UV illumination shown in Scheme 3b. Because the bottom energy level of the conduction band of ZnO is higher than the new equilibrium Fermi energy level (E_f) of Ag/ZnO, the photoexcited electrons on the conduction band could transfer from ZnO to Ag nanoparticles. Therefore, Ag nanoparticles, acting as electron sinks, reduce the recombination of photoinduced electrons and holes, and improve the photocatalytic activity. On the other hand, more Ag particles loading will cover more semiconductor surface, inhibit UV irradiation to the interface of the Ag/ZnO, besides, silver particles also act as recombination centers at high silver deposition which leads to the decrease of the photocatalytic activity.

A disadvantage of ZnO photocatalyst is the photocorrosion induced by photogenerated holes, and the stability of the ZnO NRA films is an important concern for the repeated use of the photocatalysts, so repeated photocatalytic cycling tests were carried out for our samples (Fig. 9). UV irradiation time was half an hour. Our product either ZnO or Ag/ZnO does not exhibit any great lost in activity

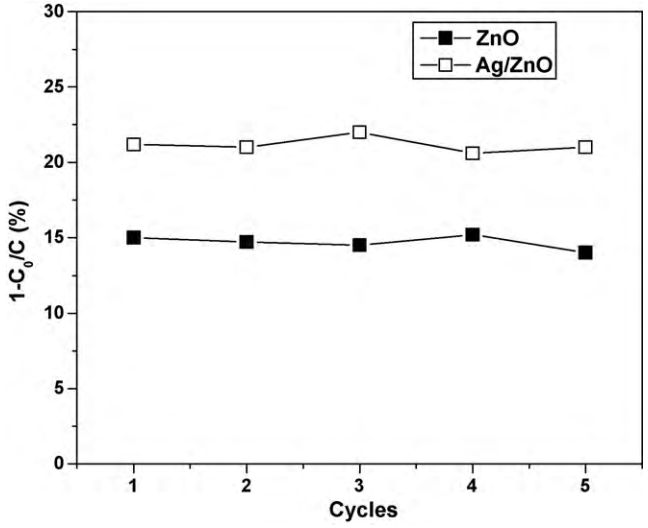

Fig. 9. Cycling runs for photodegradation of MB under UV-light irradiation. (a) ZnO NRA (solid), (b) Ag/ZnO NRA with an Ag content of 0.37 at.% (blank).

Table 1
The pseudo-first-order kinetic constant of MB photodegradation and photodegradation ratio using different photocatalysts.

Samples	Kinetics constants, k (min^{-1})	Photodegradation ratios after 1 h irradiation (%)
Pure ZnO	5.16×10^{-3}	36.2
ZnO/Ag (0.02 M)	5.69×10^{-3}	39.6
ZnO/Ag (0.05 M)	7.63×10^{-3}	49.3
ZnO/Ag (0.1 M)	7.17×10^{-3}	47.2
ZnO/Ag (0.2 M)	6.08×10^{-3}	42.6

even after five times UV-light degradation process, which were carried out by turns on the same sample in different days. However, both photocatalysis and photocorrosion are very complex processes, the detailed mechanism for the enhanced photocatalytic activity and stability of the 1D ZnO nanostructures is still an open question.

3.5. Photoluminescence properties

Photocatalytic activity is closely related with the lifetime of photogenerated electrons and holes. PL signals result from the recombination of photoinduced charge carriers, so PL measurements were carried out to confirm the charge separation behavior and efficiency in ZnO/Ag system. Fig. 10a shows the PL spectra

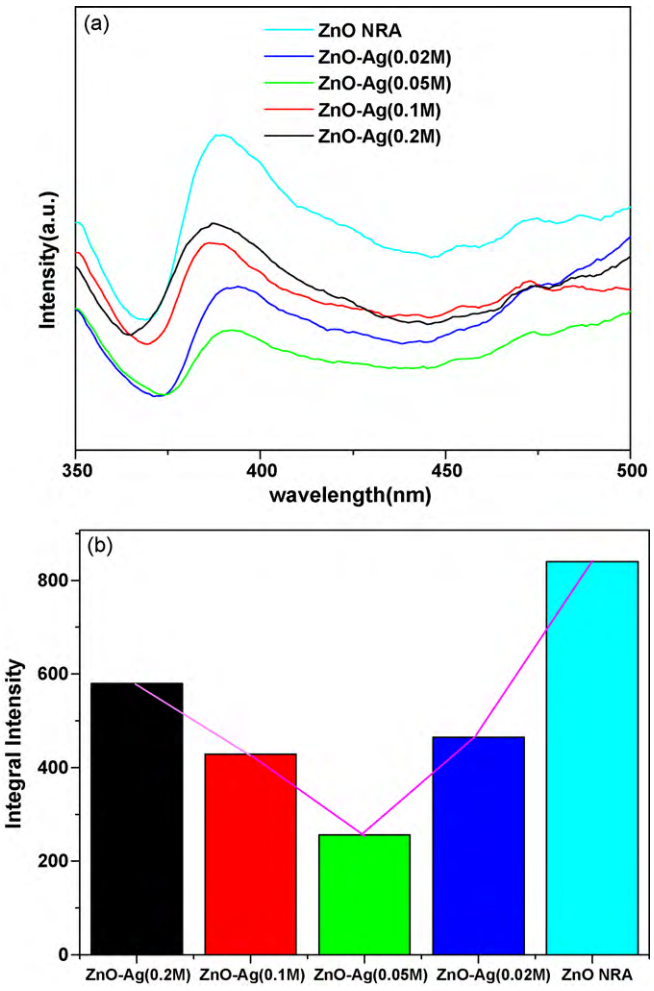

Fig. 10. (a) PL emission spectra of pure ZnO NRA, ZnO/Ag (0.02 M), ZnO/Ag (0.05 M), ZnO/Ag (0.1 M) and ZnO/Ag (0.2 M), (b) integral PL emission of pure ZnO NRA, ZnO/Ag (0.02 M), ZnO/Ag (0.05 M), ZnO/Ag (0.1 M) and ZnO/Ag (0.2 M) at the peaks of NBE emission of ZnO.

of the as-prepared ZnO and Ag/ZnO samples. It is found that all individual curves similarly show two emission bands, including a near UV emission at around 380–400 nm, corresponding to the near band edge (NBE) emission of ZnO, and a weak blue emission at about 470 nm. Fig. 10b shows the integral PL intensities at the peaks of NBE emission of ZnO. It can be seen that the PL intensities of these samples vary in the following order: pure ZnO > ZnO/Ag (0.02 M) > ZnO/Ag (0.05 M) < ZnO/Ag (0.1 M) < ZnO/Ag (0.2 M). In these samples, ZnO nanorods arrays were synthesized under the same experimental condition and the ZnO arrays had similar geometric modality, about 1.0 μm in length and about 100 nm in diameter, according to the SEM measurements. As a result, the amounts of ZnO in each sample was almost the same, the difference of PL intensities of the samples were mainly caused by the change of amount of Ag in different samples.

It is generally believed that a lower excitonic PL intensity means an enhanced separation and transfer of photoinduced electrons. Therefore, it is reasonable that the PL intensities of Ag-loaded samples were much lower than that of the sample without Ag. Compare the photocatalytic activity and PL results, we can found that the order of PL intensities of the samples was just opposite to the order of the photocatalytic activities, indicating that the charge separation effect was confirmed by PL results.

4. Conclusions

Highly ordered ZnO nanorods array grown on glass substrate was successfully modified with Ag nanoparticles using a facile photodeposition method and the optimized content of Ag deposit was obtained. On the basis of the structural characterizations and photocatalytic results, the effect of Ag deposition on the photocatalytic performance of ZnO NRA can be summarized as follows: (i) Ag deposit acted as electron sinks to enhance the separation of photoexcited electrons from holes; (ii) Ag particles also act as recombination centers at high silver deposition which leads to the decrease of the material's photocatalytic activity. And the charge separation effect was confirmed by PL results.

Acknowledgement

This work was supported by National Natural Science Foundation of China. The authors are grateful to Fanqing Li, Shuyuan Zhang, Jianxin Wu, and Chunyi Xu, Structure Research Laboratory, USTC, Hefei, for the SEM, HRTEM, XPS, and Raman data.

References

[1] N.X. Wang, C.H. Sun, Y. Zhao, S.Y. Zhou, P. Chen, L. Jiang, Fabrication of three-dimensional ZnO/TiO_2 heteroarchitectures via a solution process, J. Mater. Chem. 18 (2008) 3909–3911.
[2] S.K. Kansal, M. Singh, D. Sud, Studies on TiO_2/ZnO photocatalysed degradation of lignin, J. Hazard. Mater. 153 (2008) 412–417.
[3] H.B. Zeng, W.P. Cai, P.S. Liu, X.X. Xu, H.J. Zhou, C. Klingshirn, H. Kalt, ZnO-based hollow nanoparticles by selective etching: elimination and reconstruction of metal-semiconductor interface, improvement of blue emission and photocatalysis, ACS Nano 2 (2008) 1661–1670.
[4] T. Tan, Y. Li, Y. Liu, B. Wang, X.M. Song, E. Li, H. Wang, H. Yan, Two-step, preparation of Ag/tetrapod-like ZnO with photocatalytic activity by thermal evaporation and spluttering, Mater. Chem. Phys. 111 (2008) 305–308.
[5] A.L. Linsebigler, G.Q. Lu, J.T. Yates, Photocatalysis on TiO_2 surfaces—principles, mechanisms, and selected results, Chem. Rev. 95 (1995) 735–758.
[6] X.Z. Li, F.B. Li, Study of Au/Au^{3+}-TiO_2 photocatalysts toward visible photooxidation for water and wastewater treatment, Environ. Sci. Technol. 35 (2001) 2381–2387.
[7] H. Frenzel, A. Lajn, M. Brandt, H. von Wenckstern, G. Biehne, H. Hochmuth, M. Lorenz, M. Grundmann, ZnO metal-semiconductor field-effect transistors with Ag-Schottky gates, Appl. Phys. Lett. 92 (2008).
[8] C.P. Wu, D.Q. Yi, J. Li, L.R. Xiao, B. Wang, F. Zheng, Investigation on microstructure and performance of Ag/ZnO contact material, J. Alloys Compd. 457 (2008) 565–570.
[9] X.B. Wang, C. Song, K.W. Geng, F. Zeng, F. Pan, Luminescence and Raman scattering properties of ag-doped ZnO films, J. Phys. D: Appl. Phys. 39 (2006) 4992–4996.
[10] S.H. Jeong, B.N. Park, S.B. Lee, J.H. Boo, Structural and optical properties of silver-doped zinc oxide sputtered films, Surf. Coat. Technol. 193 (2005) 340–344.
[11] J.T. Hu, T.W. Odom, C.M. Lieber, Chemistry and physics in one dimension: synthesis and properties of nanowires and nanotubes, Acc. Chem. Res. 32 (1999) 435–445.
[12] Y.J. Lee, D.S. Ruby, D.W. Peters, B.B. McKenzie, J.W.P. Hsu, ZnO nanostructures as efficient antireflection layers in solar cells, Nano Lett. 8 (2008) 1501–1505.
[13] J.J. Qiu, W.D. Yu, X.D. Gao, X.M. Li, Sol–gel assisted ZnO nanorod array template to synthesize TiO_2 nanotube arrays, Nanotechnology 17 (2006) 4695–4698.
[14] M. Guo, P. Diao, S.M. Cai, Hydrothermal growth of well-aligned ZnO nanorod arrays: dependence of morphology and alignment ordering upon preparing conditions, J. Solid State Chem. 178 (2005) 1864–1873.
[15] M. Ohyama, H. Kozuka, T. Yoko, Sol-gel preparation of ZnO films with extremely preferred orientation along (0 0 2) plane from zinc acetate solution, Thin Solid Films 306 (1997) 78–85.
[16] J.X. Li, J.H. Xu, W.L. Dai, K.N. Fan, Dependence of Ag deposition methods on the photocatalytic activity and surface state of TiO_2 with twist like helix structure, J. Phys. Chem. C 113 (2009) 8343–8349.
[17] E. Stathatos, P. Lianos, P. Falaras, A. Siokou, Photocatalytically deposited silver nanoparticles on mesoporous TiO_2 films, Langmuir 16 (2000) 2398–2400.
[18] Y. Tak, K.J. Yong, Controlled growth of well-aligned ZnO nanorod array using a novel solution method, J. Phys. Chem. B 109 (2005) 19263–19269.
[19] L. Vayssieres, Growth of arrayed nanorods and nanowires of ZnO from aqueous solutions, Adv. Mater. 15 (2003) 464–466.
[20] R. Georgekutty, M.K. Seery, S.C. Pillai, A highly efficient Ag–ZnO photocatalyst: synthesis, properties, and mechanism, J, Phys. Chem. C 112 (2008) 13563–13570.
[21] J.J. Wu, S.C. Liu, Catalyst-free growth and characterization of ZnO nanorods, J. Phys. Chem. B 106 (2002) 9546–9551.
[22] C. Dahmen, A.N. Sprafke, H. Dieker, M. Wuttig, G. von Plessen, Optical and structural changes of silver nanoparticles during photochromic transformation, Appl. Phys. Lett. 88 (2006).
[23] K. Naoi, Y. Ohko, T. Tatsuma, TiO_2 films loaded with silver nanoparticles: control of multicolor photochromic behavior, J. Am. Chem. Soc. 126 (2004) 3664–3668.
[24] Y. Ohko, T. Tatsuma, T. Fujii, K. Naoi, C. Niwa, Y. Kubota, A. Fujishima, Multicolour photochromism of TiO_2 films loaded with silver nanoparticles, Nat. Mater. 2 (2003) 29–31.
[25] K. Matsubara, T. Tatsuma, Morphological changes and multicolor photochromism of Ag nanoparticles deposited on single-crystalline TiO2 surfaces, Adv. Mater. 19 (2007) 2802–2806.
[26] N.S. Ramgir, I.S. Mulla, V.K. Pillai, Micropencils and microhexagonal cones of ZnO, J. Phys. Chem. B 110 (2006) 3995–4001.
[27] Y.H. Zheng, L.R. Zheng, Y.Y. Zhan, X.Y. Lin, Q. Zheng, K.M. Wei, Ag/ZnO heterostructure nanocrystals: synthesis, characterization, and photocatalysis, Inorg. Chem. 46 (2007) 6980–6986.
[28] W.W. Lu, G.S. Liu, S.Y. Gao, S.T. Xing, J.J. Wang, Tyrosine-assisted preparation of Ag/ZnO nanocomposites with enhanced photocatalytic performance and synergistic antibacterial activities, Nanotechnology 19 (2008).
[29] W.W. Lu, S.Y. Gao, J.J. Wang, One-pot synthesis of Ag/ZnO self-assembled 3D hollow microspheres with enhanced photocatalytic performance, J. Phys. Chem. C 112 (2008) 16792–16800.